THE AMERICAN SOCIETY OF MECHANICAL ENGINEERS
345 E. 47th St., New York, N.Y. 10017

95-GT-435

EXPERIMENTAL STUDY OF THE UNSTEADY BOUNDARY LAYER BEHAVIOR ON A TURBINE CASCADE

M. T. Schobeiri, K. Pappu, L. Wright
Turbomachinery Performance Laboratory
Texas A&M University
College Station, Texas

ABSTRACT

The unsteady boundary layer behavior on a turbine cascade is experimentally investigated and the results are presented in this paper. To perform a detailed study on unsteady cascade aerodynamics and heat transfer, a new large-scale, high-subsonic research facility for simulating the periodic unsteady flow has been developed. It is capable of sequentially generating up to four different unsteady inlet flow conditions that lead to four different passing frequencies, wake structures, and freestream turbulence intensities. For a given Reynolds number, three different unsteady wake formations are utilized. Detailed unsteady boundary layer velocity, turbulence intensity, and pressure measurements are performed along the suction and pressure surfaces of one blade. The results presented in the temporal-spatial domain display the transition and further development of the boundary layer, specifically the ensemble-averaged velocity and turbulence intensity.

NOMENCLATURE

C = blade chord

C_p = pressure coefficient, $C_p = \dfrac{(p-p_{ref})}{\frac{1}{2}\rho V_{ref}^2}$

d = reference lateral distance from the surface, d = 5 mm

D_R = diameter of the wake generating rod

n_R = number of rods in each cluster

Re_C = Reynolds number based on the blade chord

Tu = turbulence intensity

U = rotor circumferential velocity, belt translational velocity

V = instantaneous velocity

$\bar{V}$ = time-averaged mean velocity

v = turbulent fluctuation velocity

V_{ax} = axial velocity

V_u = rotor blade tangential velocity

S_B = blade spacing

S_R = rod spacing

s = streamwise distance from the leading edge of the blade

s_0 = streamwise distance from the leading edge to the trailing edge of the blade

t = time

$\langle V \rangle$ = ensemble-averaged mean velocity

$\langle v \rangle$ = ensemble-averaged fluctuation velocity

y = lateral distance from the surface of the blade

λ = turbine stage load coefficient, $\lambda = (V_{u2}+V_{u3})/U$

τ = one wake-passing period

σ = cascade solidity, $\sigma = C/S_B$

φ = flow coefficient $\varphi = V_{ax}/U$

Ω = unsteady flow parameter, $\Omega = \dfrac{c}{S_R}\dfrac{U}{V_{ax}} = \dfrac{\sigma}{\varphi}\dfrac{S_B}{S_R}$

INTRODUCTION

The improvement of efficiency and performance of turbine and compressor stages has been one of the key issues in turbomachinery research and development for

Presented at the International Gas Turbine and Aeroengine Congress and Exposition
Houston, Texas - June 5-8, 1995

several decades. Considerable efforts have been made to develop blade profiles with optimum efficiency for a variety of specific stage-load and flow coefficients (λ, φ) that are encountered in turbine engine design technology. The optimization of blade geometry with regard to the profile loss/efficiency, incidence and deviation range by the industry and research institutions was performed utilizing steady flow cascade experiments. As a rule, the implementation of these profiles into the turbine component was associated with discrepancies in efficiency behavior which were corrected using empirical correlations. These discrepancies are partially attributed to the unsteady nature of the turbomachinery stage flow which does not exist in steady cascade measurement. The unsteady flow is induced by the alternate change of the absolute and relative frame of references represented by the stator and rotor cascades and vice-versa. Earlier experimental research work by Speidel (1957) dealt with the effect of unsteady flow on a single profile. Speidel utilized a symmetric profile and an oscillating wire for generating the unsteady flow and found a direct correlation between the Strouhal number and the profile loss coefficient. He attributed the increase of the profile loss coefficient to the decrease of the length of laminar boundary layer. Although the research facility by Speidel did not simulate the real periodic unsteady flow situation, the results indicated the significance of the unsteady flow effect on blade profile loss.

Modeling the Unsteady Flow

The significance of the unsteady flow effect on efficiency and performance of compressor and turbine stages was recognized in the early seventies by several researchers. Fundamental studies by Pfeil and Pache (1977), Pfeil and Herbst (1979), Schröder (1983), and Orth (1992), were investigating the effect of unsteady wake flow on the boundary layer transition along flat plates. Pfeil and Pache (1977) simulated the periodic unsteady inlet flow and studied its influence on boundary layer development under adverse and favorable pressure gradients. They utilized a wake generator with a series of cylindrical rods arranged circumferentially on two parallel rotating disks (squirrel cage type) positioned upstream of the test objects. Using a flat plate and a NACA-65010 airfoil as the test objects for boundary layer investigations, Pfeil and Pache (1977) concluded that the existing calculation methods based on experiments with artificially increased stochastic turbulence of external flow are poorly applicable to their test cases. In continuation of the above research work, Pfeil and Herbst (1979), Herbst (1980), and Schröder (1983) concentrated their efforts on investigating the transition process of unsteady boundary layers. Using a flat plate and varying the pressure gradient, the unsteady inlet flow condition by changing the number, diameter, and frequency of the rods, Pfeil et al. generated wake induced transition, where intermittently laminar and turbulent states of the boundary layer were observed. Their studies show that the wakes generated by the rods affect the onset and length of transition, particularly if the flow is subjected to a favorable pressure gradient. They established an unsteady boundary layer transition model, which is generally accepted. Priddy and Bayley (1988) and Liu and Rodi (1989, 1991) concentrated their efforts on heat transfer and boundary layer investigations using a similar type of wake generator. Using the flat plate data by Pfeil and Herbst, the turbine data by Dring et al. (1986), and the cascade data by Wittig et al. (1988), Mayle (1991) created a correlation for intermittency distribution.

The above boundary layer research program by Pfeil was continued very recently by Orth (1991, 1992), whose comprehensive research work deals with the boundary layer transition on a flat plate periodically disturbed by wakes. Orth found that a boundary layer flow periodically disturbed by wakes differs in two ways from a boundary layer developing in an undisturbed flow. First, an early onset of transition is observed momentarily as the high turbulence level of the wake disturbs the boundary layer and leads to the formation of turbulent patches. Second, laminar becalmed regions are formed behind the turbulent patches, so that brief periods of laminar flow are still observed beyond the location at which the steady flow boundary layer is fully turbulent.

Schobeiri and Radke (1994b) experimentally investigated the effects of periodic unsteady wake flow and pressure gradient on the boundary layer transition and development along the concave surface of a constant curvature plate. The measurements were carried out under zero and negative pressure gradients utilizing an unsteady flow research facility with a rotating cascade of rods positioned upstream of the curved plate. Boundary layer measurements with hot-wire probes were analyzed using the ensemble-averaging technique. Based on the comprehensive experimental investigations, Schobeiri and Radke concluded that the wake-induced unsteady flow significantly affects the boundary layer transition behavior leading to the formation of a primary boundary layer with quasi-steady character and a periodic unsteady secondary boundary layer, generated by the interaction of the wake strip and the wall. The onset of the primary boundary layer and the location of its high turbulence intensity core was shifted toward the plate leading edge when subjected to periodic unsteady wakes. As they pointed out, this shift was very likely due to the increased turbulence intensity of the freestream caused by the intensive mixing of the incoming wakes. The secondary

boundary layer periodically disturbed the laminar boundary layer leading to periodic transition.

Earlier investigations, by Eifler (1975) and Trost (1975), utilized a rotating cylinder cascade concept to generate periodic unsteady inlet flow upstream of an annular turbine cascade. While Eifler was primarily interested in the wake development and decay process, Trost's efforts were concentrated on the effect of the wakes on turbine cascade losses. Simoneau et al. (1984) developed a similar research facility to investigate blade heat transfer aspects under unsteady flow conditions. This facility also served to investigate the turbulence structure and wake propagation reported by Morehouse and Simoneau (1986), O'Brien and Capp (1989), and O'Brien et al. (1986). Using a similar research facility, Schultz et al. (1989) and Poensgen and Gallus (1991) investigated three-dimensional wake decay characteristics within compressor cascades. Doorly and Oldfield (1985a, 1985b), Ashworth et al. (1985, 1989), and Dullenkopf et al. (1991) applied the above concept of rotating cylinder to rectilinear turbine cascades for simulating the unsteady shock wave passing and carried out heat transfer investigations. Concerning the turbine stage, concentrated efforts to understand the effect of unsteady wake flow on the enhancement of turbine blade heat transfer coefficient has resulted in a tremendous amount of related papers (see exhaustive literature review by Mayle 1991 and Schobeiri and John 1994a). Regarding the compressor flow, efforts have been focused on understanding the effect of unsteady wake flow on performance, particularly on the flow separation, rotating stall, and surge (Schultz et. al 1990, Dong and Cumpsty 1990).

Unsteady Turbine Cascade Investigations

In spite of the above mentioned efforts, comparatively little attempts have been undertaken to investigate and to comprehend the impact of the unsteady wake flow on turbine blade aerodynamics, boundary layer transition, and efficiency. To investigate the effect of unsteady wakes on turbine blade aerodynamics, Trost (1975) utilized a rotating cylinder cascade, which was installed in front of an annular turbine cascade. Generating different turbulence levels by varying the rotational speed of the rotating cylinder, Trost measured the blade loss coefficients of three different turbine cascade types and compared them with those that were obtained from steady measurement. He found that the steady data cannot be transferred to turbine rotors. This is particularly true for cases where the turbine blade was subjected to a laminar separation. Liu and Rodi (1989) carried out boundary layer and heat transfer measurements on a turbine cascade, which was installed in the squirrel cage type wake generator discussed previously. Due to the restricted accessibility of the hot wire probe, the first 30% of both pressure and suction surfaces could not be reached. As a result, in spite of a major experimental effort, the interesting transition events could not be measured.

Unsteady Turbine Stage Investigations

Recent study by Schröder et al. (1992) underscores the significance of the influence of the periodic wake impingement on the blade aerodynamics. Referring to a series of experimental investigations, Schröder et al. (1992) conclude that the measurements taken on individual airfoils or in cascades without periodic wakes provide no conclusive evidence for the interpretation of the boundary layer transition process. In a recent experimental study on a multistage Low-Pressure (LP) turbine, Arndt (1993) illustrates the profound influence of the wake induced rotor-stator and rotor-rotor interaction on the flow through downstream blade rows. Arndt shows that the interaction results in strongly amplitude-modulated periodic and turbulent velocity fluctuations downstream of every rotor blade row. Using surface mounted hot film anemometers, Hodson et al. (1994) performed experimental investigations on a multistage LP-turbine. Based on the results, they suggest that the presence of the wake influences the transition in a separated flow region. They concluded that a LP-blade design based on steady flow methods may not represent the optimum that can be achieved.

Objective of Present Investigation

The above mentioned studies on turbine aerodynamics have largely concentrated on the measurement of blade surface properties such as the wall shear stress. The few boundary layer measurements are not comprehensive enough to provide any conclusive evidence for the interpretation of the boundary layer transition and separation processes and their direct impact on the profile loss, which is a critical parameter for blade design. The objective of this work is to provide a detailed unsteady boundary layer information essential for evaluating the impact of the unsteady wake flow on the blade efficiency.

It is well known that the boundary layer measurement is the most time consuming aerodynamic measurement. Any attempt to increase the number of parameters to be studied would inevitably result in substantial increase of the measurement time. Considering this fact and the objective formulated above, a new research facility with state-of-the-art instrumentation has been developed to study, systematically and efficiently, the influence of periodically unsteady and highly turbulent flow on turbine and

compressor cascade aerodynamics and heat transfer.

EXPERIMENTAL RESEARCH FACILITY

A large-scale, high-subsonic research facility for simulating the periodic unsteady flow has been developed to study the cascade aerodynamics and heat transfer (Fig. 1). It is capable of sequentially generating up to four different unsteady inlet flow conditions that lead to four different unsteady wake structures, passing frequencies, and freestream turbulence intensities. The test facility consists of the following components.

Air Supplier, Diffuser, Silence Chamber, Nozzle

A large centrifugal fan serves as the air supplier with a volume flow rate of 15 m^3 driven by a 110 kW motor. This is capable of generating a maximum mean velocity of approximately 100 m/s at the test section inlet which corresponds to a high subsonic Mach number of $M = 0.6$ for a turbine cascade with an acceleration ratio of $V_2/V_1 = 2$. Variations of the flow velocity and Reynolds number can be achieved by operating a throttle located at the fan exit or by varying the fan speed. To protect the hot wire system, the flow entering the fan passes through a 50 mm thick fiber-glass filter capable of filtering particles of up to 5 μm. A diffuser of length 1500 mm and an area ratio of 1:4.75 is located downstream of a straight pipe that connects the diffuser with the fan. The settling chamber is made of four sections of length 900 mm and cross section of 1500 mm x 900 mm. Five screens and one honeycomb flow straightener are used to control the flow uniformity and turbulence level within the settling chamber. The first screen is placed at the diffuser exit to reduce the scale of the vortices generated by the diffuser vanes. A 50 mm wide honeycomb flow straightener with a cell size of 6 mm is located between the first two settling chamber sections. Directly downstream of the honeycomb is the second screen. This honeycomb-screen combination results in a much lower exit turbulence level than a honeycomb alone, since the large scale jets exiting from the honeycomb cells are broken up into smaller scale eddies. The other three screens are located downstream of the second, third, and fourth settling chamber sections.

Downstream of the settling chamber is a nozzle, with an area ratio of 6.75:1, that accelerates the flow to the required velocity before it enters the wake generator. The nozzle, with the exit cross section of 1000.0 x 200.0 mm, establishes a smooth transition of the flow from the settling chamber to the wake generator. With this tunnel configuration, it was possible to achieve, at the nozzle exit, a constant mean fluctuation velocity over a wide velocity range. For a nozzle exit velocity of 30 m/s, a turbulent intensity of $Tu = 0.75\%$ was measured. Subsequent measurements with higher velocities resulted in a decrease of the turbulence intensity.

Unsteady Inlet Wake Flow Generator

Two-dimensional periodic unsteady inlet flow is simulated by the translational motion of a wake generator (see Fig. 1), with a series of cylindrical rods that are attached to two parallel operating timing belts driven by an electric motor. The belts, having a length of 5000 mm, span over five shaft-pulleys arranged around the cascade test section. The drive pulley also controls the belt tension. To simulate the wake width and spacing that stem from the trailing edge of rotor blades, the diameter and number of rods can be varied. The rod diameter can vary from 2.0 - 10.0 mm. The rod spacing can be changed by attaching or detaching the rods to or from the belts. As shown in Fig. 1, the belt-pulley system is driven by an electric motor with a maximum power of 10 kW and a frequency controller. The controller allows the belts to run with a translational speed of up to 25 m/s. Considering the length and the speed of the belts, special attention had to be paid to the dynamics of the system design to avoid belt flutter and system vibration. The wake-passing frequency is monitored by a fiber-optic sensor. The sensor also serves as the triggering mechanism for data transfer and its initialization, which is required for ensemble-averaging.

Sequential Generation of Unsteady Wakes

The special design of the facility and the length of the belts enable considerable reduction of the measurement time, when performing the boundary layer experiments. If, for example, the wake spacing is the parameter to be varied, then up to four clusters of rods with constant diameter may be attached to the belts. The cylindrical rods within each cluster have the same spacing. So, it is possible to measure sequentially the effect of four different spacings at a single boundary layer point. Similarly, keeping the rod spacing constant, four different clusters each with a given rod diameter may be attached to the belt to investigate the effect of wake thickness. To clearly define the influence domain of each individual cluster with the other one, the clusters are arranged with certain distance between each other. Using the triggering system mentioned above and a continuous data acquisition, the buffer zones between the data clusters are clearly visible. The data analysis program cuts the buffer zones and evaluates the data pertaining to each cluster. Comprehensive preliminary measurements were carried out to make sure that the data were exactly

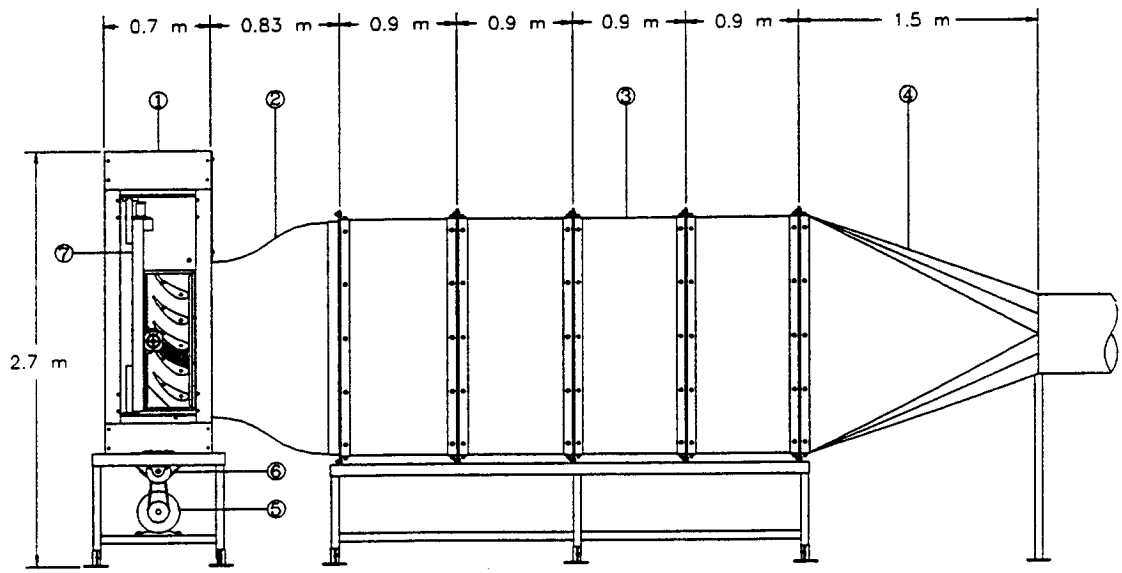

(a) Test facility

(c) Pressure tap blade

(d) Boundary layer measurement channel

(b) Test section

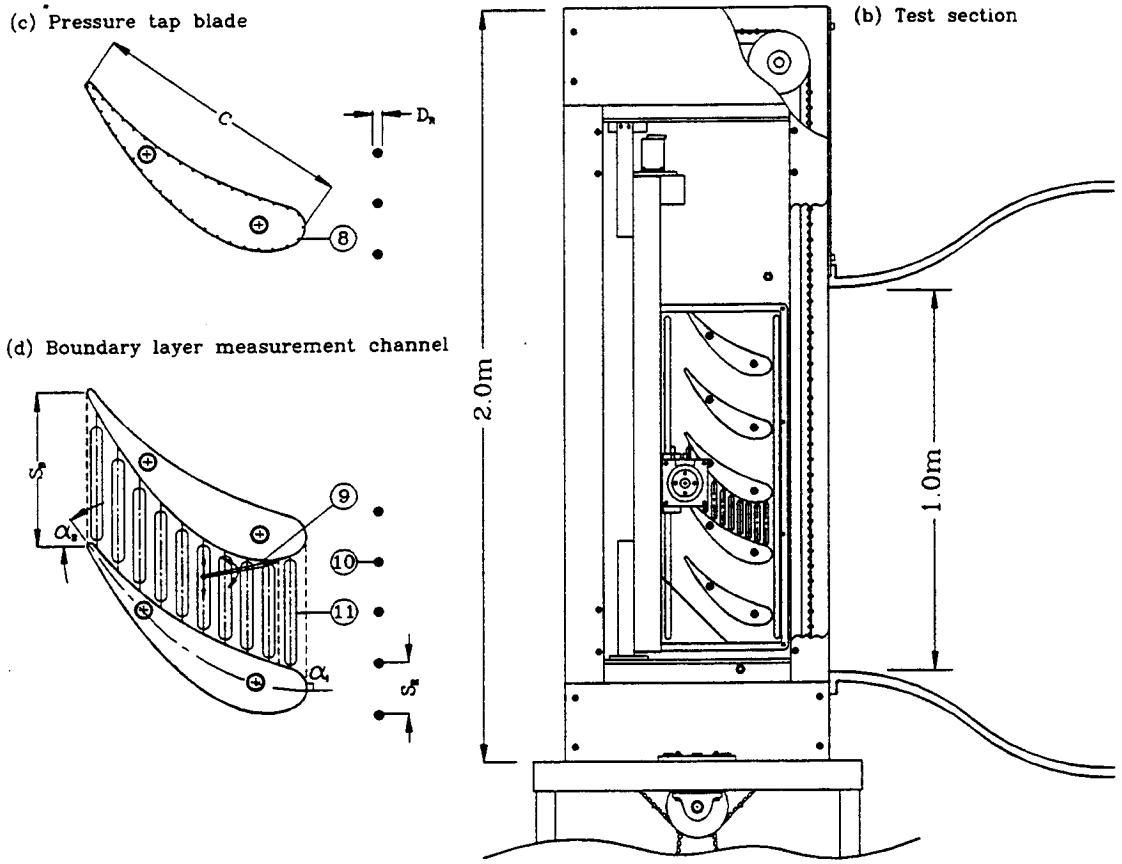

FIG. 1 TEST FACILITY: 1-TEST SECTION; 2-NOZZLE; 3-SETTLING CHAMBER; 4-DIFFUSER; 5-MOTOR; 6-BELT; 7-TRAVERSING SYSTEM; 8-STATIC PRESSURE TAPS; 9-BOUNDARY LAYER PROBE; 10-WAKE GENERATING RODS; 11-SLOTS FOR LONGITUDINAL TRAVERSE OF THE PROBE

identical to those, when the entire belt length was attached with rods of constant spacing, which corresponded to each individual cluster spacing.

Cascade Test Section

The cascade test section, shown in Fig. 1, is located downstream of the wake generator. Using the existing nozzle with a height of 1000.0 mm and width of 200.00 mm, the test section can include up to 7 blades with a height of 200.00 mm and the chord up to 250.00 mm. The blades are inserted between two vertical plexiglass side walls. One sidewall integrates the boundary layer, the inlet, and the exit traversing slots (see probe traversing). The opposite wall incorporates a specially designed traversing system for measuring the wake propagation with X-probes. For boundary layer investigations, five NASA turbine blades were implemented whose geometry is described in the NASA Report by Schobeiri et al. (1991). One of the blades was specially manufactured for the measurement of pressure distribution.

Probe Traversing System

A computer controlled traversing system is used for measuring the inlet and exit flow velocities, angles, and turbulence intensities as well as the boundary layers on suction and pressure sides. The traversing system is vertically mounted on the plexiglass side wall. It consists of a slider and a lead screw which is connected to a d.c. stepper motor with encoder and decoder. It receives signals from a computer and is driven by a FORTRAN code, with an arbitrary traversing schedule as an input, and turns the lead screw by the exact number of pulses required. An optical encoder connected to the traversing system provides a continuous feedback to the stepper motor for accurate positioning of the probes. The system is capable of traversing in small steps with a minimum of 2.5 μm, which is specifically required for boundary layer investigations, where the measurement of the laminar sublayer is of particular interest.

The boundary layer flow is measured by a single hot-wire probe using the vertical traversing system. The precise positioning of the probe relative to the blade surface is done by adjusting the zero point of the traversing schedule as close as 0.001 mm to the wall.

INSTRUMENTATION, DATA ACQUISITION, AND DATA REDUCTION

The data acquisition system is controlled by a 486-personal computer that includes a 16 channel, 12-bit analog-digital (A/D) board with 8-channel simultaneous sample and hold. Mean velocities and turbulent fluctuations are obtained using a commercial 3-channel (TSI), constant temperature hot-wire anemometer system. The system has a signal conditioner with a variable low pass filter and adjustable gain. The first channel of the anemometer is connected to a single hot-film probe or boundary layer probe while the second and third channels are connected to a X-film probe for the measurement of time dependent velocity, Reynolds stress distributions within the blade channel outside the boundary layer, turbulence intensity, and angle distribution measurements. These channels will also be used for the measurement of exit flow velocity, turbulence intensity, and angle distribution measurements.

The three channels of the anemometer are connected to the first three channels of the A/D board from which the data is sampled by the computer. A Prandtl probe, placed upstream of the diffuser, monitors the reference velocity at a fixed location. The pneumatic probes are connected with high precision differential pressure transducers for a 2-channel digital readout. A thermocouple is placed downstream of the test section to constantly monitor the flow temperature. The wake generator speed and the passing frequency signals of the rods are transmitted by a fiber-optic trigger sensor. The passage signals of the rods are detected by the sensor using a silver-coated reflective paint on one of the belts. This sensor gives an accurate readout of the speed of the wake generator and the passing frequency of the rods. The signals of the pressure transducers, thermocouple, and trigger sensors are transmitted to the A/D board and are sampled by the computer. Two adjacent blades are used for boundary layer measurement. A third blade was instrumented with 40 static pressure taps, distributed on suction and pressure surfaces. The taps were connected to a scanivalve, which sequentially transferred the pressure signals to one of the transducers that was connected to the A/D board.

In order to ensure a high level of accuracy, the calibration method and the facility described in John and Schobeiri (1993) was used for all hot-wire calibrations. The instantaneous velocity components are calculated from the temperature compensated instantaneous voltages by using the calibration coefficients. The instantaneous velocity can be represented in the following form.

$$V = \bar{V} + v \tag{1}$$

Where $\bar{V}$ is the mean (time-averaged) velocity and v is the turbulent fluctuation component. The mean velocity, also known as the time-average, is given by:

$$\bar{V} = \frac{1}{N}\sum_{j=1}^{N} V_j \tag{2}$$

where N = 16384 is the total number of samples at one boundary layer location. A sampling rate of 1000 Hz was used for investigating the steady flow (no wakes). The root mean square value of the turbulent velocity fluctuation is obtained from the instantaneous and mean velocities by:

$$v = \sqrt{\frac{1}{N}\sum_{j=1}^{N}(V_j - \bar{V})^2} \tag{3}$$

and the local turbulence intensity is defined as:

$$Tu_{loc} = \frac{v}{\bar{V}}\times 100 = \frac{1}{\bar{V}}\sqrt{\frac{1}{N}\sum_{j=1}^{N}(V_j - \bar{V})^2} \times 100 \tag{4}$$

The unsteady data were reduced by the ensemble-averaging method. At each boundary layer position, 2048 samples were taken at a sampling rate of 2874 Hz for each of 100 revolutions of the wake generator. The data were ensemble-averaged with respect to the rotational period of the wake generator. Before final data were taken, number of samples per revolution and total number of revolutions were varied to determine the optimum settings for convergence of the ensemble-average.

The ensemble-averaged fluctuation velocity and the turbulence intensity were calculated from the instantaneous velocity samples by:

$$\langle V_i(t_i)\rangle = \frac{1}{N}\sum_{j=1}^{N} V_{ij}(t_i) \tag{5}$$

$$\langle v_i(t_i)\rangle = \sqrt{\frac{1}{N}\sum_{j=1}^{N}\left[V_{ij}(t_i) - \langle V_i(t_i)\rangle\right]^2} \tag{6}$$

$$\langle Tu_i(t_i)\rangle = \frac{\langle v_i(t_i)\rangle}{V_{ref}}\times 100 \tag{7}$$

where j=1,2,...N, and N is the total number of periods (i.e. 100 revolutions), and i=1,2,...,m, where m is the number of samples taken per period (m=2048). V_{ref} is the reference velocity for the particular boundary layer traverse.

The ensemble-averaged boundary layer parameters such as displacement thickness $\langle\delta_1\rangle$, momentum thickness $\langle\delta_2\rangle$, and shape factor $\langle H_{12}\rangle$ are calculated as follows:

$$\langle\delta_1\rangle = \int_0^{\langle\delta\rangle}\left(1 - \frac{\langle V\rangle}{\langle V\rangle_e}\right) dy \tag{8}$$

$$\langle\delta_2\rangle = \int_0^{\langle\delta\rangle}\frac{\langle V\rangle}{\langle V\rangle_e}\left(1 - \frac{\langle V\rangle}{\langle V\rangle_e}\right) dy \tag{9}$$

$$\langle H_{12}\rangle = \frac{\langle\delta_1\rangle}{\langle\delta_2\rangle} \tag{10}$$

EXPERIMENTAL RESULTS AND DISCUSSION

To investigate the influence of unsteady wake flow on boundary layer development along the suction and pressure surfaces of the turbine blades specified in Table 1, three clusters of cylindrical rods with diameter D_R = 5 mm were attached to the two belts of the wake generator. This cylinder diameter was chosen to fulfil the similarity criterion that requires the generation of a drag coefficient C_D (see Eifler (1975) for details) that is approximately equal to the C_D of the turbine blade with the chord and spacing given in Table 1. For the flow condition given in Table 1, detailed boundary layer measurements were performed. The diameter of the rods of all the three clusters, given in Table 1, is the same and is selected based on the approximate drag coefficient value that pertains to the equivalent profile.

Surface Pressure Distribution

The pressure distribution, shown in Fig. 2, was taken by a multi-channel scanivalve for a steady (Ω = 0.0) and an unsteady case, where rods with one uniform spacing of S_R = 160 mm, corresponding to Ω = 0.822, were attached to the whole length of the belt. The pressure signals inherently signify the time-averaged pressure because of the internal pneumatic damping effect of the connecting pipes to the transducer. The noticeable deviation in pressure distribution between the steady and unsteady cases, especially on the suction surface, is due to the drag of the bars adding transverse momentum to the flow. No pressure measurements were taken for the current configuration of the belt with three clusters of rods since these measurements would not reflect the true values that would correspond to each individual cluster because of the averaging of pneumatic signals by the scanivalve.

The time-averaged pressure coefficient along the pressure and suction surfaces is plotted in Fig. 2. On the suction surface (lower portion) the flow first accelerates sharply, reaches a minimum pressure coefficient at $s/s_0 \approx 0.25$ and then continuously decelerates at a moderate rate until the

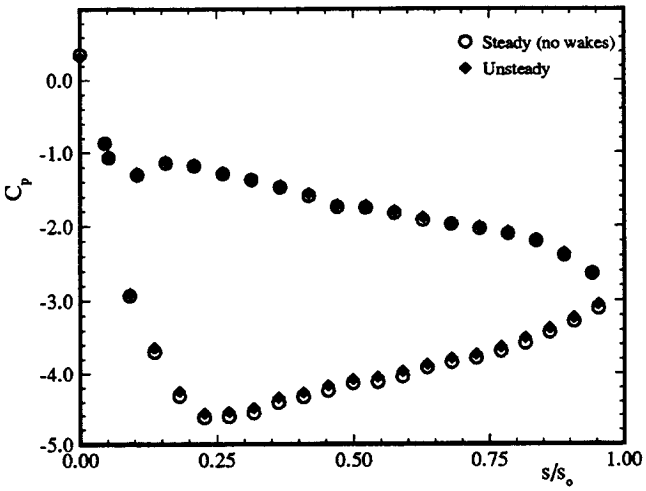

FIG. 2 PRESSURE DISTRIBUTION AT Re_c = 264187

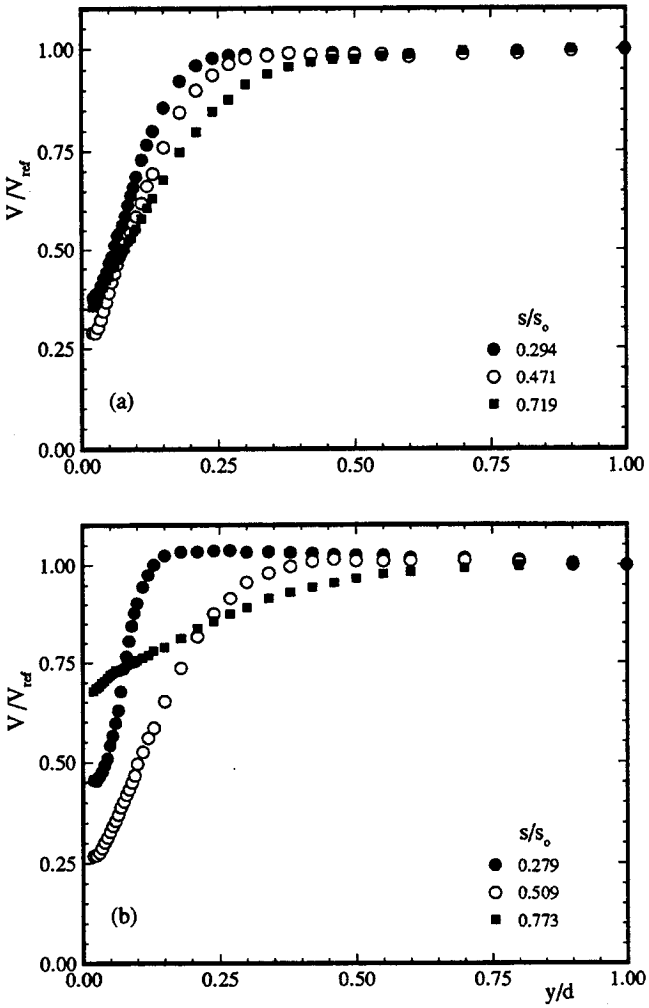

FIG. 3 NONDIMENSIONAL MEAN VELOCITY FOR DIFFERENT STREAMWISE POSITIONS ON (a) PRESSURE AND (b) SUCTION SURFACES

trailing edge is reached. On the pressure surface, the flow accelerates, reaches a minimum pressure coefficient at $s/s_0 \approx 0.1$, and experiences a short deceleration and then accelerates almost continuously at a slower rate. This pressure distribution indicates that the flow on both the surfaces, except for a short distance around $s/s_0 \approx 0.1$, is subjected to a negative pressure gradient until $s/s_0 \approx 0.25$ is reached. Beyond this point, the pressure gradient on the pressure surface remains negative, while on the suction surface, positive pressure gradient prevails. This pressure gradient situation has a very significant effect on the boundary layer development, as we will see later in the corresponding section of this paper.

Boundary Layer Velocity and Turbulence Fluctuation Distributions

Boundary layer profiles were first taken for steady inlet flow condition (no wake present) on the suction surface at 13 streamwise positions and on the pressure surface at 11 streamwise positions. In each of the Figs. 3(a) and 3(b), three velocity profiles are plotted that reflect the representative boundary layer behavior on both the surfaces. The boundary layer profiles and integral parameters for the steady flow serve as the reference case for comparison with the unsteady cases presented below.

Periodic unsteady flow was established by the wake generator, which included three clusters of cylindrical rods that were attached to the timing belts running with a translational speed of U = 7.0 m/s. To account for the unsteadiness caused by the frequency of the individual wake generating clusters and their spacing, the flow velocity, and the cascade parameters, we define an unsteady flow parameter $\Omega = \frac{c\ U}{S_R\ V_{ax}} = \frac{\sigma\ S_B}{\varphi\ S_R}$ that includes the cascade solidity σ, the flow coefficient φ, the blade spacing S_B, and the rod spacing S_R. The individual cluster configurations with the corresponding Ω - parameter are specified in Table 1. Experimental investigations were performed for four different unsteady flow parameter values of Ω = 0.0, 0.822, 1.644, 3.288. These values cover the entire reduced frequency range encountered in turbomachinery. Since the results for Ω = 1.644 with the rod spacing S_R = 80 mm are very similar to those of Ω = 0.822 (rod spacing S_R = 160 mm), they are not presented in this paper.

Figure 4 displays the temporal distribution of the ensemble-averaged boundary layer velocity <V> for three representative streamwise positions, s/s_o, at y = 2.5 mm above the pressure surface for those two Ω - values discussed earlier. The choice of the lateral location y = 2.5

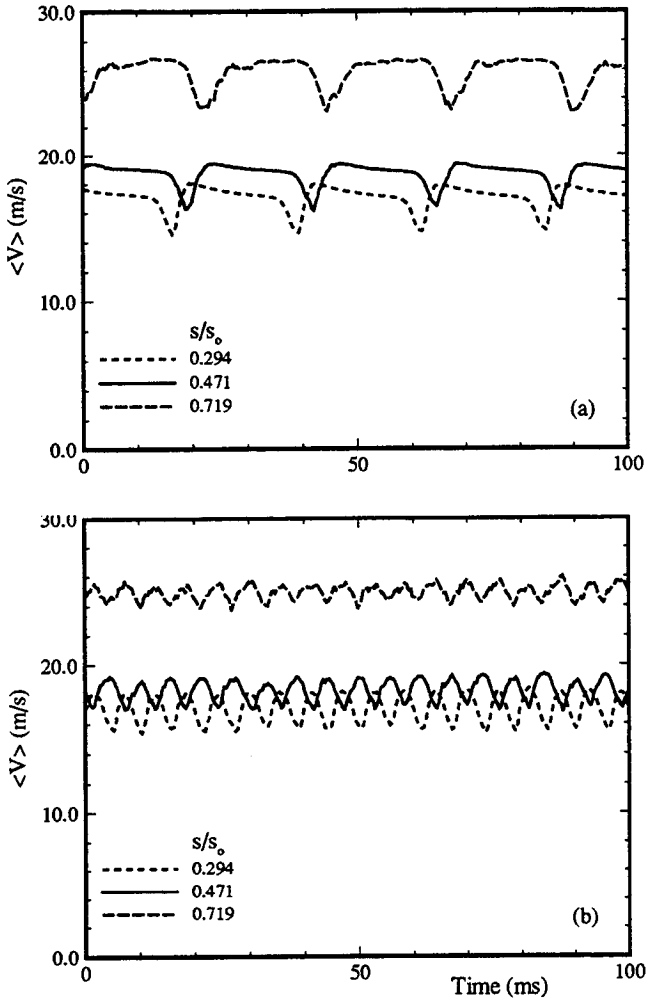

FIG. 4 ENSEMBLE-AVERAGED VELOCITY DISTRIBUTION ON PRESSURE SURFACE AT y = 2.5 mm FOR (a) Ω = 0.822 AND (b) Ω = 3.288

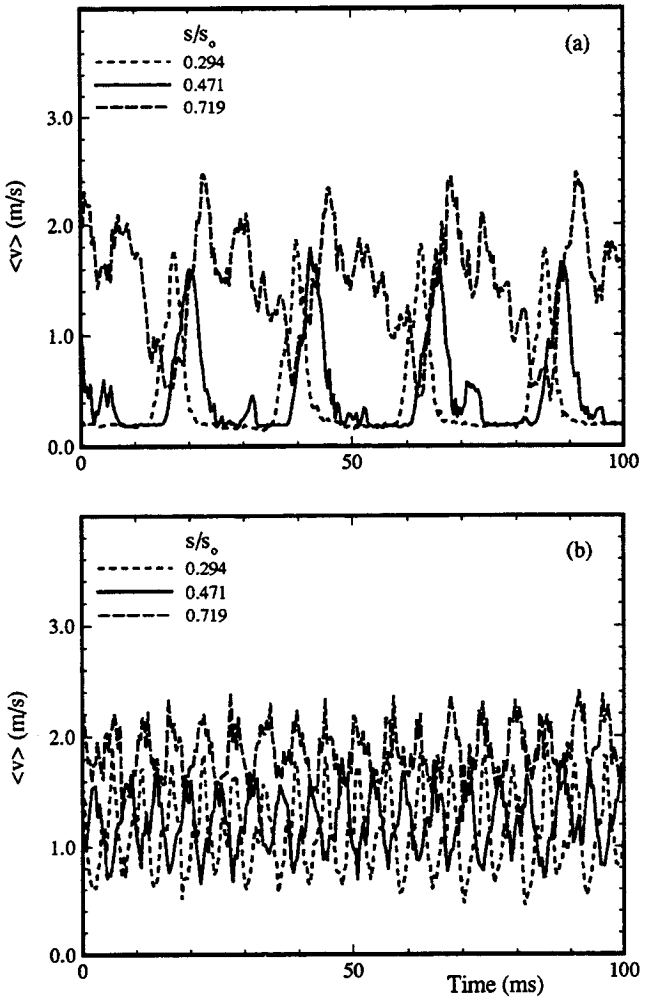

FIG. 5 ENSEMBLE-AVERAGED RMS VELOCITY DISTRIBUTION ON PRESSURE SURFACE AT y = 2.5 mm FOR (a) Ω = 0.822 AND (b) Ω = 3.288

mm is arbitrary, and for most streamwise positions, it lies in the boundary layer except near the leading edge. For the first half of the profile length, s/s_0= 0.294 and 0.471, the velocity distributions in Fig. 4(a) exhibit an asymmetric behavior indicating the effect of a strong curvature. By convecting further downstream, the diminishing curvature effect, starting at s/s_0 = 0.719, results in an almost symmetric velocity profile. In recent comprehensive theoretical and experimental studies, Schobeiri et al. (1994) investigated the effect of curvature on the steady and unsteady turbulent wake structure and velocity distribution. In a parallel study, Schobeiri and Radke (1994b) performed detailed boundary layer measurements along a curved plate. In both cases, they observed similar asymmetric behavior of the velocity distributions. They argued that the asymmetric pattern is due to the non-zero pressure gradient in lateral direction that is characteristic of curved channels. By entering a flow channel, where the lateral pressure gradient approaches a zero value, the asymmetric behavior diminishes. This is clearly shown in the studies by Herbst (1980), Schröder (1985), Liu and Rodi (1991), and recently by Orth (1991, 1992). They performed unsteady boundary layer transition studies along flat plates inside straight channels, where they measured fully symmetric ensemble-averaged velocity distributions. The continuous acceleration of the velocity reflects the channel contraction. Further increasing the value of the Ω -parameter results in higher frequency (Fig. 4b) and lower amplitude of the ensemble-averaged velocity. Considering the ensemble-averaged RMS-distributions (Figs. 5(a,b)) for the above velocity distributions, it is seen that outside the wakes at lower Ω -values within the first half of the profile, very low

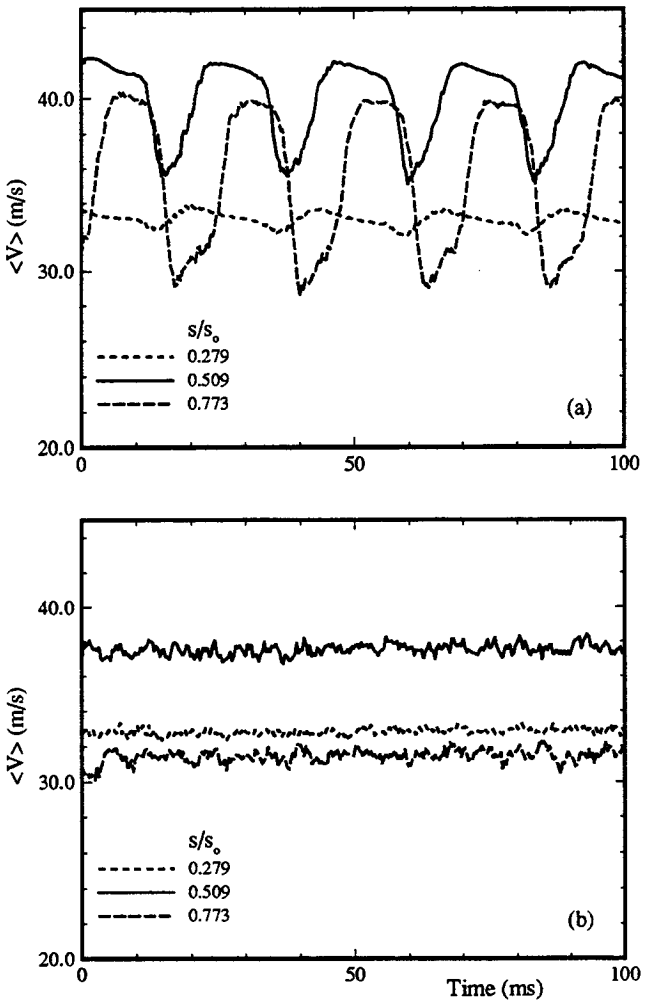

FIG. 6 ENSEMBLE-AVERAGED VELOCITY DISTRIBUTION ON SUCTION SURFACE AT y = 2.5 mm FOR (a) Ω = 0.822 AND (b) Ω = 3.288

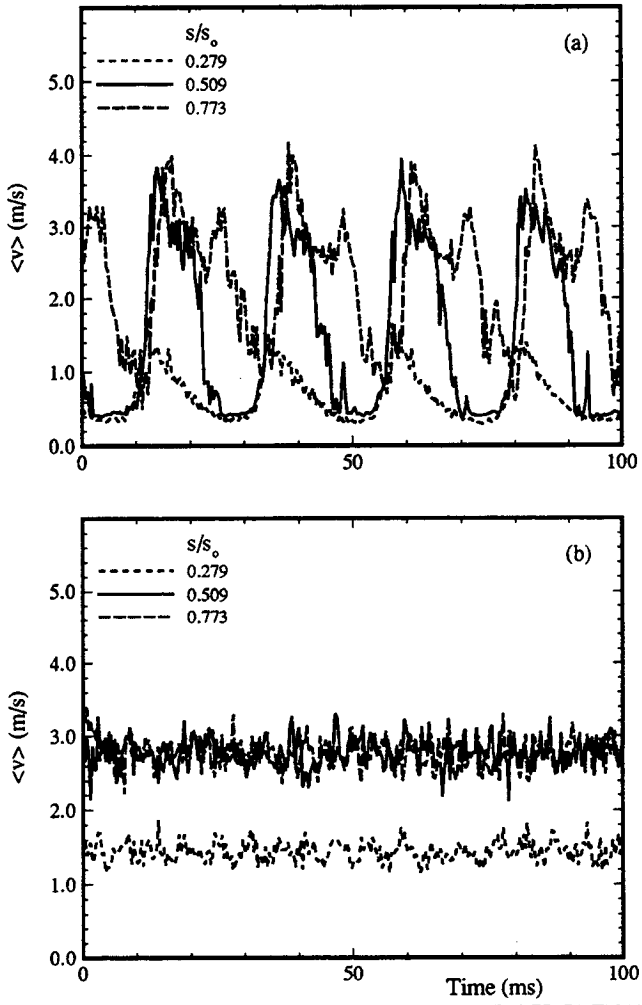

FIG. 7 ENSEMBLE-AVERAGED RMS VELOCITY DISTRIBUTION ON SUCTION SURFACE AT y = 2.5 mm FOR (a) Ω = 0.822 AND (b) Ω = 3.288

amplitude and low frequency of turbulent fluctuations exist. This pattern changes drastically (Fig. 5b) when the cascade is subjected to a higher unsteadiness (Ω = 3.288). In this case, the amplitude and the frequency of the fluctuations increase substantially. This phenomenon is typical for LP-stages (see previous discussion of Arndt's paper).

Figure 6 shows the temporal distribution of the ensemble-averaged boundary velocity <*V*> for three representative streamwise positions, s/s_0, at $y = 2.5$ mm above the suction surface for the same two Ω - values discussed above. Starting with $s/s_0 = 0.279$, the velocity distribution (small-dashed line in Fig. 6a) exhibits an asymmetric behavior with low velocity defect indicating the strong mixing effect due to the high negative pressure gradient on the suction surface. By convecting further downstream, the boundary layer flow on the suction surface undergoes a positive pressure gradient (see also the pressure distribution, Fig. 2) that leads to the recovery of the wake flow at $s/s_0 > 0.279$. Further increasing the value of the Ω - parameter to 1.644 results in almost symmetric velocity profiles with higher frequency and slightly lower amplitude of the ensemble-averaged velocity. The deterministic periodic character of the velocity fully diminishes by further increasing the value of the Ω - parameter (Fig. 6b). The velocity profile apparently assumes a stochastic pattern indicating the strong interaction of the wakes that results in a complete mixing and decay of the wake. Once a complete mixing has been reached, the frequency and the amplitude of the periodic velocity fluctuations assume order of magnitudes that are comparable to those of the turbulent fluctuations (compare Figs. 6b and 7b). This phenomenon is characteristic for a multi-stage turbine, where the upstream wakes continuously

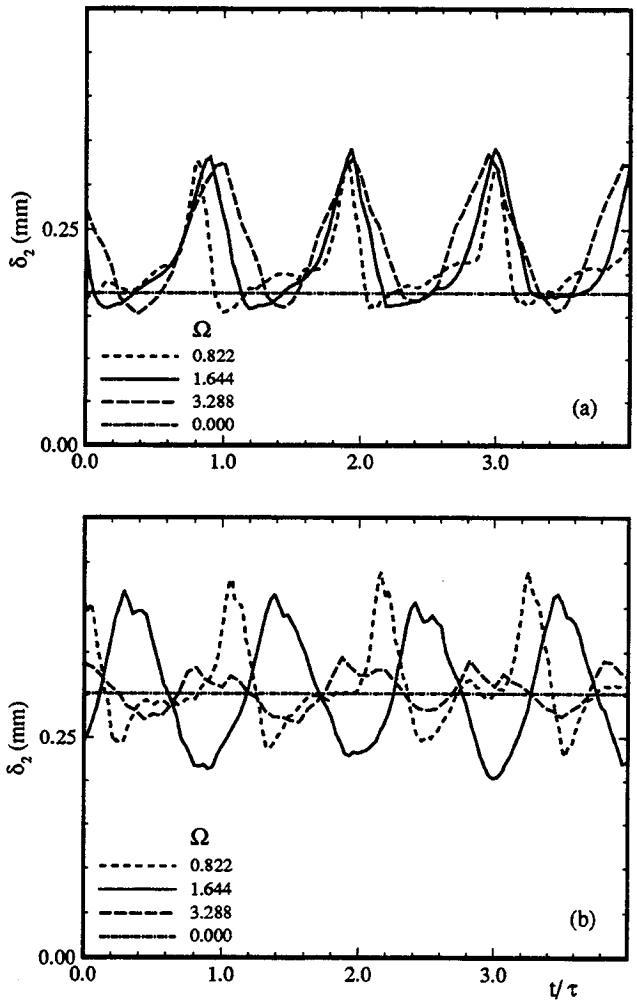

FIG. 8 ENSEMBLE-AVERAGED MOMENTUM THICKNESS DISTRIBUTION ON PRESSURE SURFACE AT (a) s/s_0 = 0.294 AND (b) s/s_0 = 0.719

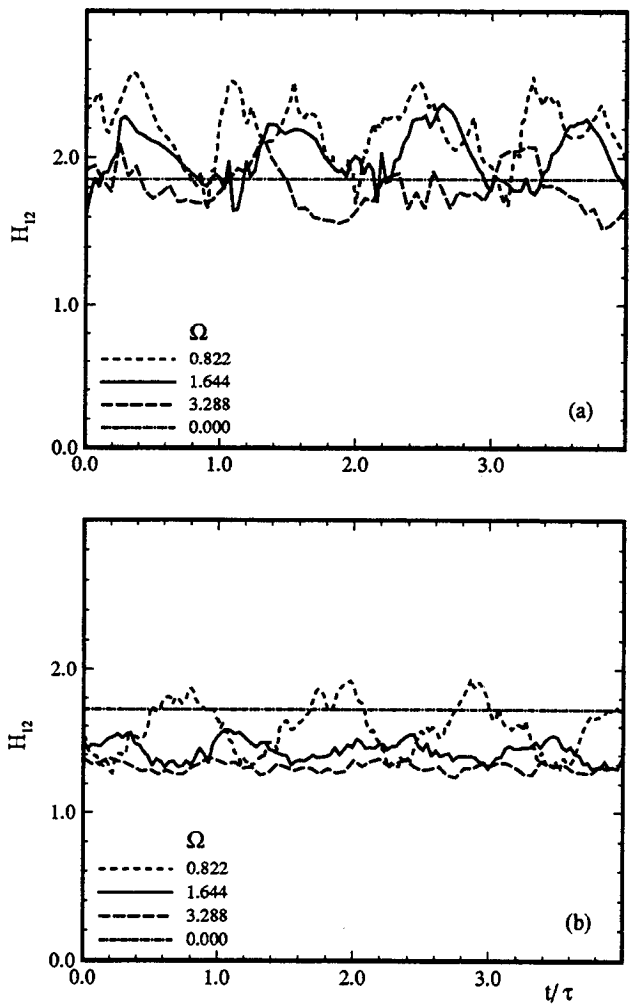

FIG. 9 ENSEMBLE-AVERAGED SHAPE FACTOR DISTRIBUTION ON PRESSURE SURFACE AT (a) s/s_0 = 0.294 AND (b) s/s_0 = 0.719

propagate downstream and mix with the downstream wakes resulting in a strong mixing process (see Arndt's paper). The behavior of ensemble-averaged RMS-distributions (Figs. 7(a,b)) is similar to the previous case (Figs. 5(a,b)) and does not need to be further discussed.

Boundary Layer Ensemble and Time Averaged Integral Quantities

The integral parameters such as momentum thickness and shape factor are of particular interest to a turbine designer, since they provide an accurate first estimation of the quality of the designed blade. The ensemble-averaged distributions of the momentum deficiency thickness and shape factor for the pressure and suction surfaces are represented in Figs. 8 to 11 for two representative s/s_0 positions at four different Ω - values that include the steady flow with $\Omega = 0$. The period τ represents the wake-passing period specific to the individual wake generating cluster, which is characterized by the Ω - value under investigation. The periodic behavior of the ensemble-averaged momentum thickness as a result of the embedded periodic wake flow is clearly visible for both pressure and suction surfaces (Figs. 8(a,b) and 10(a,b)). On the first half of the pressure surface (Fig. 8a, s/s_0 = 0.294), the minima of $\langle\delta_2\rangle$ for three non-zero Ω - values are approximately equal to the momentum thickness of the steady case with $\Omega = 0$. This value approximately corresponds to the momentum thickness of a fully laminar flow at the above given s/s_0 position. By moving downstream, $\langle\delta_2\rangle$ experiences a continuous increase, where its time-averaged value approaches the steady case ($\Omega = 0$) value. The shape factor $\langle H_{12}\rangle$ experiences a similar

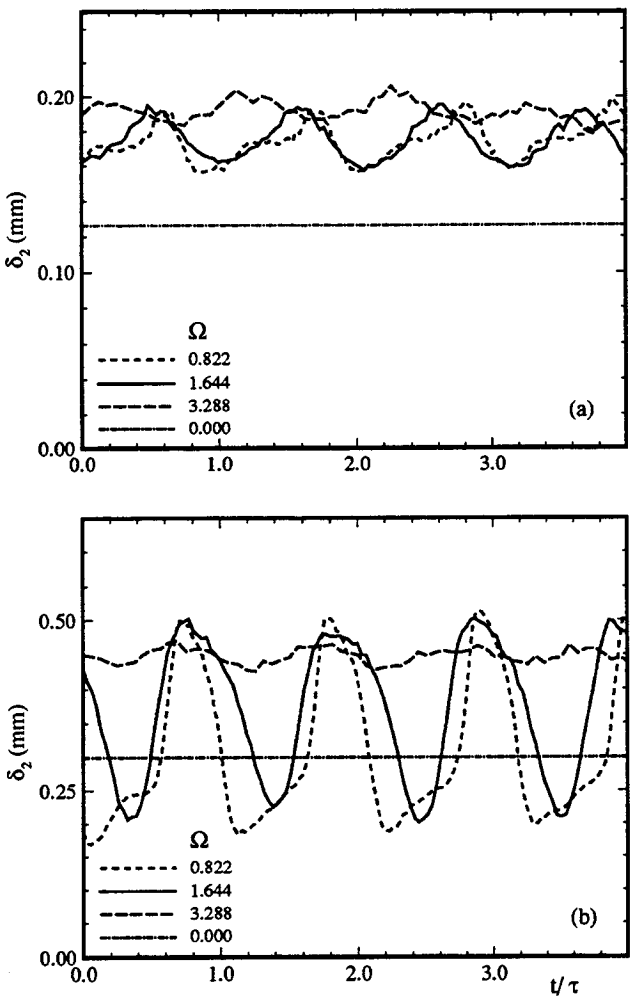

FIG. 10 ENSEMBLE-AVERAGED MOMENTUM THICKNESS DISTRIBUTION ON SUCTION SURFACE AT (a) s/s_0 = 0.138 AND (b) s/s_0 = 0.509

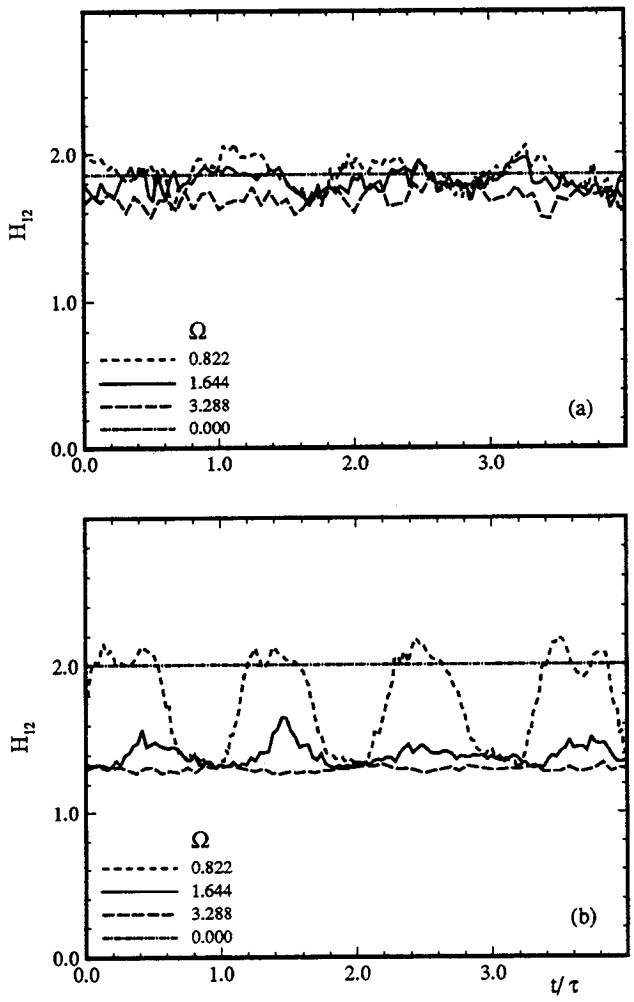

FIG. 11 ENSEMBLE-AVERAGED SHAPE FACTOR DISTRIBUTION ON SUCTION SURFACE AT (a) s/s_0 = 0.138 AND (b) s/s_0 = 0.509

periodic change with an average below the steady case as shown in Figs. 9(a,b) and 11(a,b). With increasing Ω - value, the time dependent distribution of the shape factor approaches a constant value which is far below the value measured for steady case on the pressure side (Fig. 9). The slight aperiodicity in $\langle H_{12} \rangle$ distributions could be due to the sensitivity of $\langle \delta_1 \rangle$ and $\langle \delta_2 \rangle$ to the calculation of $\langle \delta \rangle$. Other information regarding the overall evaluation of turbine blade is provided by the time-averaged momentum thickness as shown in Figs. 12(a,b) for pressure and suction surfaces. The time-averaged momentum thickness indicates that for the particular blade under investigation, an increase of unsteady parameter Ω results in a consistent augmentation of the momentum thickness over the entire pressure and suction surfaces with the exception of the location s/s_0 = 0.97 for the suction surface. The higher δ_2 value for Ω = 1.644 may be attributed to the sensitivity of δ_2 calculation with regard to the calculation of the boundary layer thickness δ. Although a general conclusion cannot be drawn from these results, they evidence the impact of unsteady wake flow on the boundary parameter and thus the profile loss coefficient and efficiency. This clearly shows that the steady state data cannot be transferred to the unsteady turbine design technology without modifications.

Steady Boundary Layer, Contour Plots

Figure 13 shows the contour plots of the reference turbulence intensity distribution on both pressure and suction surfaces, where the reference velocity, V_{ref}, is equal to the velocity at 5 mm above the plate surface for each longitudinal position. These contour plots serve as the

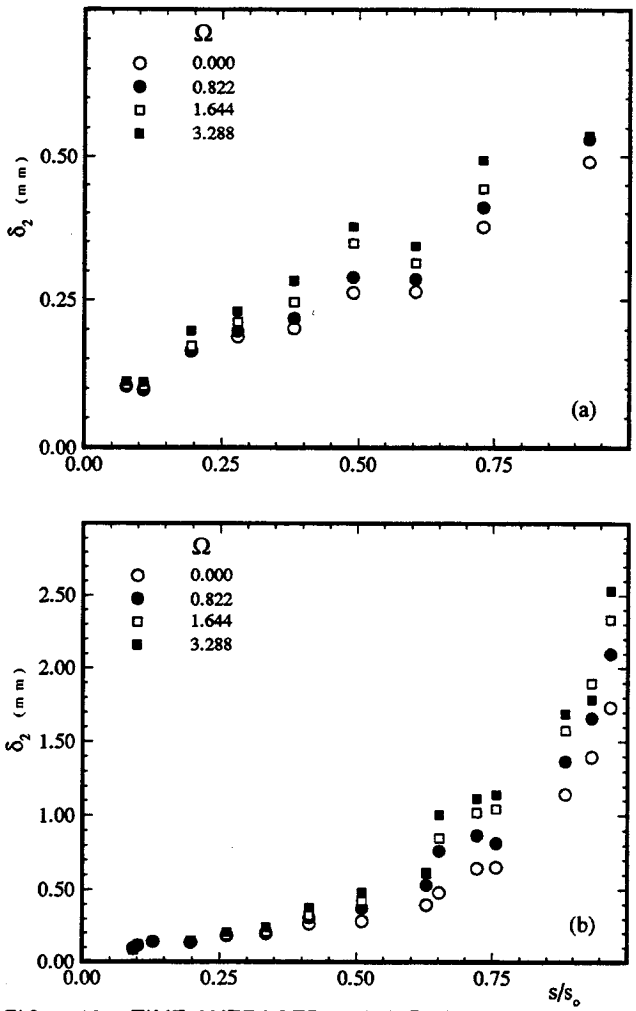

FIG. 12 TIME-AVERAGED MOMENTUM THICKNESS DISTRIBUTION ON (a) PRESSURE AND (b) SUCTION SURFACES

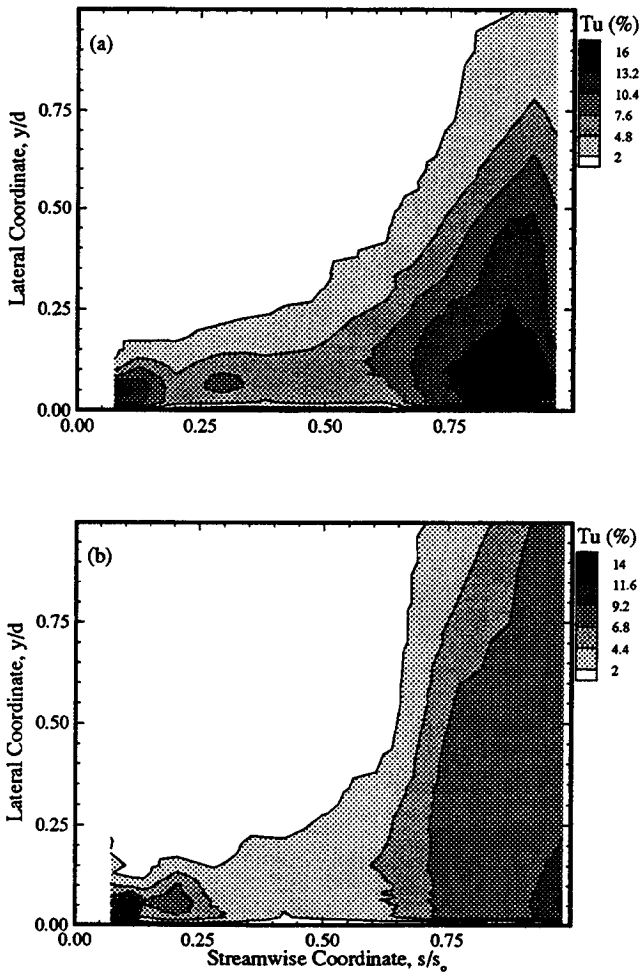

FIG. 13 TIME-AVERAGED REFERENCE TURBULENCE INTENSITY FOR STEADY FLOW CASE ON (a) PRESSURE AND (b) SUCTION SURFACES

reference profiles for comparison purposes discussed below. On the pressure surface, a region of high turbulence intensity (10%-13%) can be observed that has a compact peak core (Fig. 13a), which starts at s/s_0 = 0.72 with a lateral extension of y/d = 0.25 with d = 5.0 mm. However, on the suction surface, the region of high turbulence intensity (9%-12%) has the peak core (Fig. 13b) that starts at s/s_0 = 0.92. The use of high turbulence intensity cores of comparable turbulence level allows a more precise comparison as the exact location of laminar-turbulent transition is always associated with uncertainty, particularly for thin boundary layers.

Periodic Unsteady Boundary Layer, Contour plots

Figures 14 and 15 show the contour plots of the time-averaged reference turbulence intensity on pressure and suction surfaces for two different Ω - values under investigation. As can be seen from Fig. 14(a), the high turbulence intensity core of above 10% starts at s/s_0 = 0.62 for Ω = 0.822 with a lateral extension of y/d = 0.3 with d = 5 mm. Using the longitudinal extension of this high intensity core as a basis, and comparing with the steady case (Fig. 13a) suggests that the periodic unsteady flow has caused a shift of transition onset towards the leading edge. Further increase in Ω (Fig. 14b) caused the high turbulence intensity cores to advance further toward the leading edge with corresponding decrease in lateral extension, revealing the effect unsteadiness as to cause earlier transition. Similar observations can be drawn from the time-averaged contour plots on the suction surface, shown in Figs. 15(a,b). The time-averaged turbulence intensity contours serve for global

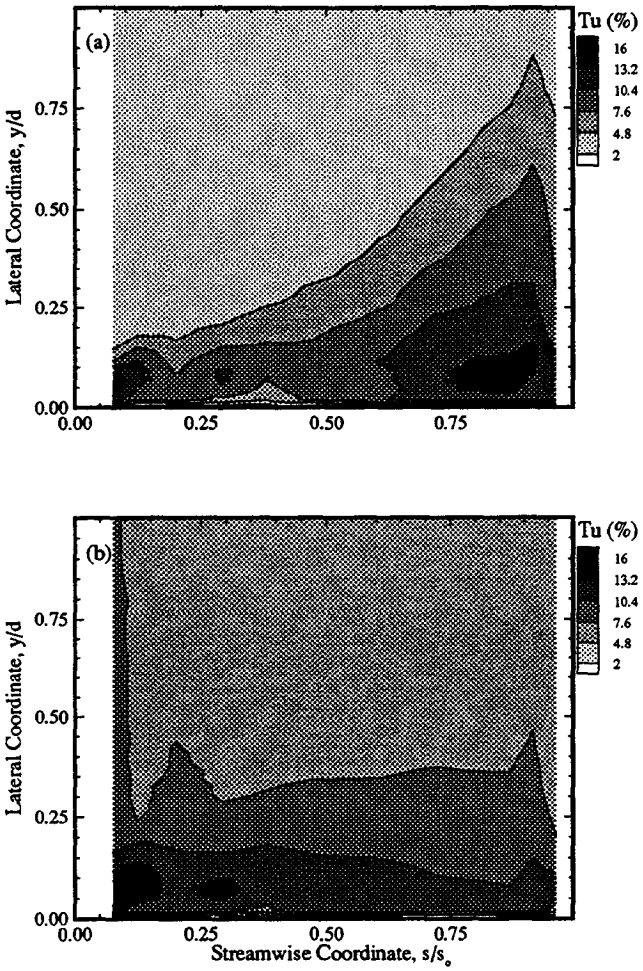

FIG. 14 TIME-AVERAGED REFERENCE TURBULENCE INTENSITY CONTOURS FOR UNSTEADY FLOW CASE ON PRESSURE SURFACE AT (a) Ω = 0.822 AND (b) Ω = 3.288

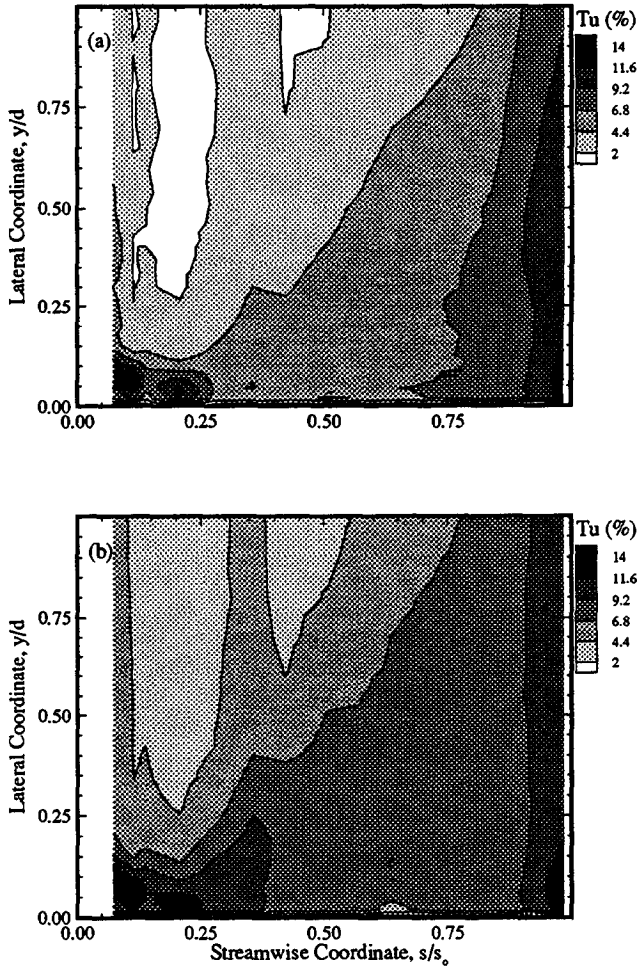

FIG. 15 TIME-AVERAGED REFERENCE TURBULENCE INTENSITY CONTOURS FOR UNSTEADY FLOW CASE ON SUCTION SURFACE AT (a) Ω = 0.822 AND (b) Ω = 3.288

comparison purposes only and do not include the important unsteady details.

The temporal-spatial distribution of the ensemble-averaged turbulence intensity for a lateral position of y = 0.75 mm on both the pressure and suction surfaces for different Ω - values is shown in Figs. 16 and 17. As shown in Fig. 16(a), the boundary layer is periodically disturbed by the wakes that produce high turbulence intensity cores and extended becalmed regions. These regions are observed between the blade leading edge and the streamwise position of $s/s_0 = 0.7$ for Ω = 0.822. Increasing Ω to 3.288 causes an earlier mixing of the impinging wakes that finally leads, for the suction surface, to a complete degeneration of the deterministic periodic wake flow into a stochastic turbulent flow. The existence of becalmed regions was discussed in detail by Schobeiri and Radke (1994b). Such becalmed regions are not clearly distinguishable for the case of Ω = 3.288 (Fig. 16b), representing highest wake passing frequency, where the flow is highly turbulent all along the blade surfaces. The results for the suction surface, shown in Figs. 17(a,b), can be interpreted similarly. A comparison of the pressure and suction surface turbulence intensity contour plots, Figs. 16(a) and 17(a), indicates that the wake on the suction surface generates a higher turbulence intensity starting at $s/s_0 \approx 0.25$ which coincides with the pressure minimum on the suction surface (Fig. 2). From Fig. 17(a), it is clear that the wake trailing edge, which is convecting downstream with lower velocity, does not have sufficient momentum to overcome the positive pressure gradient that prevails downstream of the pressure minimum. This leads to stronger velocity deformation and thus stronger dissipation that results in narrower becalmed

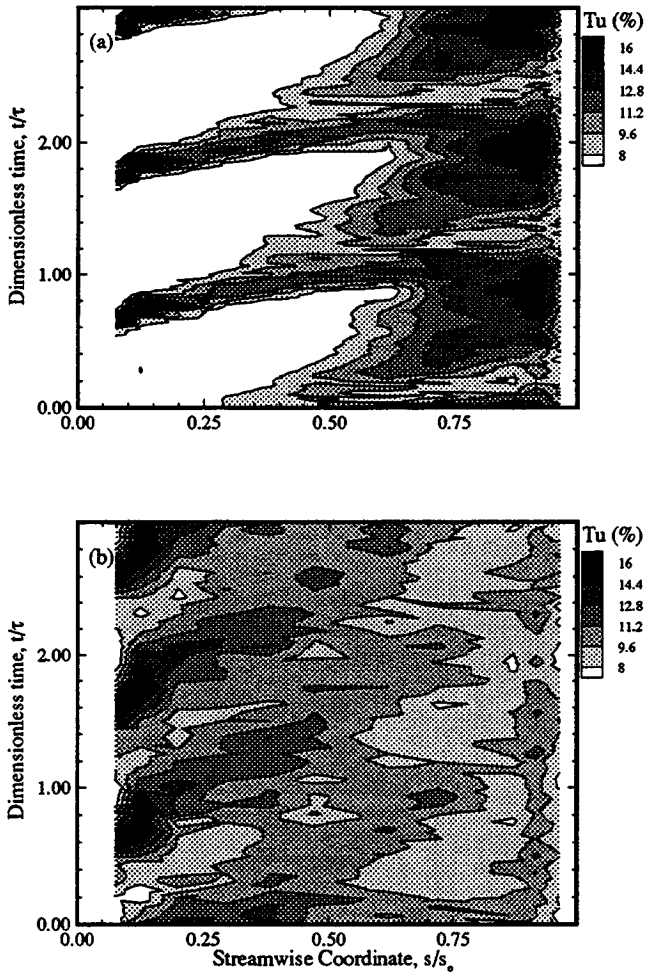

FIG. 16 ENSEMBLE-AVERAGED TURBULENCE INTENSITY IN TEMPORAL-SPATIAL DOMAIN ON PRESSURE SURFACE AT y = 0.75 mm FOR (a) Ω = 0.822 AND (b) Ω = 3.288

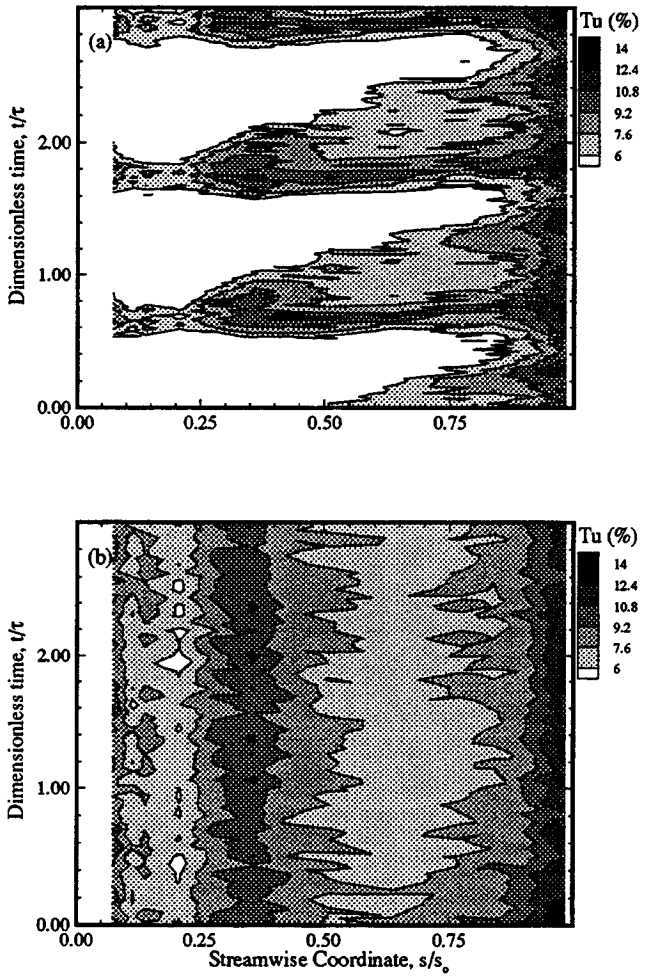

FIG. 17 ENSEMBLE-AVERAGED TURBULENCE INTENSITY IN TEMPORAL-SPATIAL DOMAIN ON SUCTION SURFACE AT y = 0.75 mm FOR (a) Ω = 0.822 AND (b) Ω = 3.288

region compared to the pressure surface.

CONCLUSIONS

A detailed experimental study of the behavior of the unsteady boundary layer of a turbine cascade was presented. One steady and three different unsteady inlet wake flow conditions with the corresponding passing frequencies, wake structures, and freestream turbulence intensities were investigated utilizing a new large-scale, high-subsonic research facility, which was specially designed for simulating the periodic unsteady flow within HP, IP, and LP-turbines. The three unsteady flow conditions were sequentially generated by three clusters of rods with the same diameter. The clusters were attached to two parallel timing belts with translational motion. The results of the comprehensive unsteady boundary layer measurements were presented in time-averaged, ensemble-averaged, and contour plot forms. The pressure distribution on the pressure side indicated a continuous acceleration of the flow, while on the suction side the initially strong acceleration was followed by a continuous mild decelaration that significantly influenced the unsteady boundary layer state. The unsteady wake flows characterized by the periodic asymmetric velocity distributions were clearly differentiable for small Ω - values. Doubling Ω from 0.822 to 1.644 resulted in higher turbulence intensity outside the wake. Further increase of Ω caused an earlier mixing of the impinging wakes that finally lead, for the suction surface, to a complete degeneration of the deterministic periodic wake flow into a stochastic turbulent flow. The time-averaged integral

TABLE 1: SPECIFICATIONS OF INLET FLOW, BLADE, CASCADE, AND WAKE GENERATOR CHARACTERISTICS

Parameters	Values	Parameters	Values
Axial velocity	V_{ax} = 15 m/s	Inlet turbulence intensity	Tu = 0.8%
Blade inlet flow angle	$\alpha_1 = 0°$	Blade exit metal angle	$\alpha_2 = 61.8°$
Blade height	L = 200.0 mm	Blade spacing	S_B = 159.31 mm
Blade chord	C = 281.8 mm	Blade Re - number	Re_c = 264,187
Cascade solidity	$\sigma = 1.76$	Cascade flow coefficient	$\varphi = 2.14$
Steady reference point (no rods)	$S_R = \infty$ mm	Ω - parameter steady case	$\Omega = 0.0$
Cluster 1 rod spacing	S_R = 160.0 mm	Ω - parameter for cluster 1	$\Omega = 0.822$
Cluster 2 rod spacing	S_R = 80.0 mm	Ω - parameter for cluster 2	$\Omega = 1.644$
Cluster 2 rod spacing	S_R = 40.0 mm	Ω - parameter for cluster 3	$\Omega = 3.288$
Rod diameter	D_R = 5.0 mm	No. of rods in cluster 2	$n_R = 19$
No. of rods in cluster 1	$n_R = 11$	No. of rods in cluster 3	$n_R = 38$

quantities indicated that for the particular blade under investigation, an increase of unsteady parameter Ω resulted in augmentation of the momentum deficiency thickness over the entire blade surface. The contour plots presented exhibited a clear picture of the unsteady boundary layer development indicating the effect of periodic wake flow, wake induced transition, and decay/mixing process that cause the final boundary layer transition.

REFERENCES

Arndt, N., 1993, "Blade Row Interaction in a Multistage Low Pressure Turbine," ASME *Journal of Turbomachinery*, Vol. 115, pp. 137-146.

Ashworth, D. A., LaGraff, J. E., Schultz, D. L., Grindrod, K. J., 1985, "Unsteady Aerodynamic and Heat Transfer Processes in Transonic Turbine Stage," ASME Paper 85-GT-128.

Ashworth, D. A., LaGraff, J. E., Schultz, D. L., 1989, "Unsteady Interaction Effects on a Turbine Blade Boundary Layer," ASME *Journal of Turbomachinery*, Vol. 111, pp. 162-168.

Doorly, D. J., Oldfield, M. L. G., 1985a, "Simulation of Wake Passing in a Stationary Turbine Rotor Cascade," *Journal of Propulsion*, Vol. 1, pp. 316-318.

Doorly, D. J., Oldfield, M. L. G., 1985b, "Simulation of the Effects of Shock Wave on a Turbine Rotor Blade," ASME Paper No. 85-GT-112.

Dong, Y., Cumpsty, N.A., 1990, "Compressor Blade Boundary Layers: Part 1- Test Facility and Measurement With No Incident Wakes," ASME *Journal of Turbomachinery*, Vol. 112, pp. 231-240.

Dong, Y., Cumpsty, N.A., 1990, "Compressor Blade Boundary Layers: Part 2-Measurement With Incident Wakes," ASME *Journal of Turbomachinery*, Vol. 112, pp. 222-230.

Dring, R. P., Blair, M. F., Joslyn, H. D., Power, G. D., Verdon, J. M., 1986, "The Effect of Inlet Turbulence and Rotor/Stator Interactions on the Aerodynamics and Heat Transfer of a Large Scale Rotating Turbine Model," NASA CR 4079.

Dullenkopf, K., Schultz, A., Wittig, S., 1991, "The Effect of Incident Wake Conditions on the Mean Heat Transfer of an Airfoil," ASME *Journal of Turbomachinery*, Vol. 113, pp. 412-418.

Eifler, J., 1975, "Zur Frage der freien turbulenten Strömungen, insbesondere hinter ruhenden und bewegten Zylindern," Dissertation D-17, Technische Hochschule Darmstadt, Germany.

Herbst, R., 1980, "Entwicklung von Strömungsgrenzsschichten bei instationärer Zuströmung in Turbomaschinen," Dissertation D-17, Technische

Hochschule Darmstadt Germany.

Hodson, H.P., Huntsman, I., Steele, A.B., 1994, "An Investigation of boundary layer development in Multistage LP-Turbine," ASME *Journal of Turbomachinery*, Vol. 116, pp. 375-383.

John, J., Schobeiri, T., 1993, "A Simple and Accurate Method for Calibrating X-Probes," Being printed in the ASME Transactions, *Journal of Engineering Fluid Engineering*.

Liu, X., Rodi, W., 1989, "Measurement of Unsteady Flow Over and Heat Transfer From a Flat Plate," ASME Paper No. 89-GT-2.

Liu, X., Rodi, W., 1991, "Experiments on Transitional Boundary Layers with Wake-Induced Unsteadiness," *Journal of Fluid Mechanics, Vol. 231 pp. 229-256.*

Mayle, R. E., 1991, "The Role of Laminar-Turbulent Transition in Gas Turbine Engines," ASME Paper No. 91-GT-261.

Morehouse, K. A., and Simoneau, R. J., 1986, "Effect of a Rotor Wake on the Local Heat on the Forward Half of a Circular Cylinder," Proceedings of the Eighth International Heat Transfer Conference, San Francisco, California, pp. 1249-1255.

O'Brien, J. E., Simoneau, R. J., LaGraff, J. E., and Morehouse, K. A., 1986, "Unsteady Heat Transfer and Direct Comparison to Steady State Measurements in a Rotor-Wake Experiment," Proceedings of the Eighth International Heat Transfer Conference, San Francisco, California, pp. 1243-1248.

O'Brien, J. E., Capp, S. P, 1989, "Two-Component Phase-Averaged Turbulent Statistics Downstream of a Rotating Spoked-Wheel Wake Generator," ASME *Journal of Turbomachinery*, Vol. 111, No. 4, pp. 475-482.

Orth, U., 1991, "Entwicklung des instationären Nachlaufs hinter quer zur Strömungsrichtung bewegten Zylindern und dessen Einfluß auf das Umschlagverhalten von ebenen Grenzschichten stromabwärts angeordneter Versuchskörper," Dissertation D-17, Technische Hochschule Darmstadt.

Orth, U., 1992, "Unsteady Boundary Layer Transition in Flow Periodically Disturbed by Wakes," ASME Paper 92-GT-283.

Poensgen, C., Gallus, H. E., 1991, "Three-Dimensional Wake Decay Inside of a Compressor Cascade and Its Influence on the Downstream Flow Field: Part I-Wake Decay Characteristics in the Flow Passage," ASME *Journal of Turbomachinery*, Vol. 113, pp. 180-189.

Poensgen, C., Gallus, H. E., 1991, "Three-Dimensional Wake Decay Inside of a Compressor Cascade and Its Influence on the Downstream Flow Field: Part II-Unsteady Flow Field Downstream of the Stator," ASME *Journal of Turbomachinery*, Vol. 113, pp. 190-197.

Pfeil, H., Pache, W., 1977, "Messungen von Strömungsgrenzschichten unter Turbomaschinenbedingungen," *Zeitschrift für Flugwissenschaften und Weltraumforschung 1*, Heft 4, pp. 267-278.

Pfeil, H., Herbst R., 1979 "Transition Procedure of Instationary Boundary Layers," ASME Paper No. 79-GT-128.

Pfeil, H., Herbst, R., Schröder, T., 1983, "Investigation of the Laminar Turbulent Transition of Boundary Layers Disturbed by Wakes," ASME *Journal of Engineering for Power*, Vol. 105, pp. 130-137.

Priddy, W. J., Bayley, F. J., 1988, "Turbulence Measurement in Turbine Blade Passage and Implications for Heat Transfer," ASME *Journal of Turbomachinery*, Vol. 110/73.

Schobeiri, M. T., McFarland, E., Yeh, F., 1991, "Aerodynamics and Heat Transfer Investigations on a High Reynolds Number Turbine Cascade," NASA TM-103260

Schobeiri, M. T., John, J. 1994a, "A Study of the Development of Steady and periodic Unsteady Turbulent Wakes Through Curved Channels at Positive, Zero and negative Pressure Gradient," NASA Final Report, Part I, NAG 3-1256.

Schobeiri, M. T., Radke, R. E., 1994b, "Effects of Periodic Unsteady Wake Flow and Pressure Gradient on Boundary Layer Transition along the Concave Surface of a Curved Plate," Presented at the International Gas Turbine and Aeroengine Congress and Exposition, The Hague, Netherlands, 94-GT-327.

Schröder, T., Baier, R.D., Broichausen, K., 1992, "Laminar Flow and Unsteady Phenomena in Boundary layers of Turbomachinery Blades," DGLR-Bericht 92-06, pp. 201-211.

Schultz, H. D., Gallus, H. E., Lakshminarayana, B., 1989, "Three-Dimensional Separated Flow Field in the Endwall Region of an Annular Compressor Cascade in Presence of Rotor-Stator Interaction, Part II: Unsteady Flow and pressure Field," ASME Paper No. 89-GT-77.

Simoneau, R. J., Morehouse, K. A., Van Fossen, G. J., Behnin, F. P., 1984, "Effect of a Rotor Wake on Heat Transfer From a Circular Cylinder," NASA TM 83613.

Speidel, L., 1957, "Beeinflussung der laminaren Grenzschicht durch periodische Störung der Zuströmung", *Zeitschrift für Flugwissenschaften* 5 heft 9, pp. 270-275.

Trost, N., 1975, "Einfluß der Zuströmturbulenz auf die Strömung in Axialgittern," Dissertation D-17, Technische Hochschule Darmstadt, Germany.

Wittig, S., Schultz, A., Dullenkopf, K., Fairbank, J., 1988, "Effects of Free-Stream Turbulence and Wake Characteristics on the Heat Transfer Along a Cooled Gas Turbine Blade," ASME Paper No. 88-GT-179.